Modern Physics Letters A
Vol. 37, No. 13 (2022) 2250079 (17 pages)
© World Scientific Publishing Company
DOI: 10.1142/S0217732322500791

World Scientific
www.worldscientific.com

Calculations of GDR parameters for deformed nuclei using LogitBoost classifier and artificial neural network

Yiğit Ali Üncü

Department of Biomedical Equipment Technology, Vocational School of Technical Sciences, Akdeniz University, Antalya 07070, Turkey
yuncu@akdeniz.edu.tr

Taner Danışman

Engineering Faculty, Department of Computer Engineering, Akdeniz University, Antalya 07190, Turkey
tdanisman@akdeniz.edu.tr

Hasan Özdoğan*

Department of Medical Imaging Techniques, Vocational School of Health Services, Antalya Bilim University, Antalya 07070, Turkey
hasan.ozdogan@antalya.edu.tr

Received 16 November 2021
Revised 1 April 2022
Accepted 20 April 2022
Published 25 May 2022

Photo-nuclear interactions are important for investigating fundamental nuclear physics phenomena. The photo-absorption cross-section energy curve displays a wide resonance called giant dipole resonance (GDR) until 30 MeV. First, spherical and deformed nuclei have been determined by using LogitBoost classifier, and then GDR parameters for deformed nuclei have been estimated by using an artificial neural network (ANN) via Levenberg–Marquardt algorithm which has been selected for the training section. In the last step, $^{233}\mathrm{U}(\gamma,\mathrm{n})^{232}\mathrm{U}$, $^{234}\mathrm{U}(\gamma,\mathrm{n})^{233}\mathrm{U}$, $^{235}\mathrm{U}(\gamma,\mathrm{n})^{234}\mathrm{U}$, $^{236}\mathrm{U}(\gamma,\mathrm{n})^{235}\mathrm{U}$, $^{238}\mathrm{U}(\gamma,\mathrm{n})^{237}\mathrm{U}$ reaction cross-sections have been computed by using GDR parameters obtained ANN estimations. The mean square error, root mean square error, and R are evaluated as the best performance of ANN estimates. Photo-neutron cross-section results have been compared with experimental data from the literature. Consequently, it has been found that ANN algorithms can be used to determine the GDR parameters for deformed nuclei in the lack of experimental data of photo-absorption reaction.

Keywords: GDR parameters; deformed nuclei; LogitBoost classifier; artificial neural networks; TALYS 1.95.

*Corresponding author.

1. Introduction

The giant dipole resonance (GDR) is the name given to the broad peak which appears in γ-ray absorption cross-sections of nuclei. GDR mechanism dominates up to 30 MeV photon energy. In the GDR region, photo-proton production, which needs to overcome the large Coulomb barrier, has lower possibility than photo-neutron production. Therefore, photo-absorption cross-section approximations can be used for photo-neutron cross-section calculations. There is a peak of photo-neutron generation for the (γ, n) reaction (different isotopes at particular energy), which is called the GDR peak energy.[1,2] Except for very light nuclei, the absorption cross-section as a function of photon energy is explained by the Lorentzian function, which shape depends on the deformation states of nuclei (for spherical nuclei (single component) or deformed nuclei (multi-component)). The photo-absorption cross-section in the GDR region is calculated by Eq. (1) where σ represents the maximum cross-section data (barn and mbarn); E_i is the photon energy belonging to the maximum cross-section value and Γ refers to the full-width-half-maximum (FWHM).[3]

$$\sigma_{\mathrm{GDR}} = \sum_{i=1} \frac{\sigma_i E_\gamma^2 \Gamma_i^2}{(E_\gamma^2 - E_i^2)^2 + E_\gamma^2 \Gamma_i^2}, \tag{1}$$

where i represents deformation status of nuclei (for spherical nuclei $i = 1$). For deformed nuclei, whose deformation parameter $\beta_2 > 0.064$, GDR region has two humps. GDR parameters for deformed nucleus can be calculated using systematic equations as shown in the following equation:[4]

$$\begin{aligned} E_2 &= 50A^{-0.232}, \\ \ln(E_2/E_1) &= 0.946\beta_2, \\ \Gamma_1 &= (0.283 - 0.263\beta_2)E_1, \\ \Gamma_2 &= (0.35 - 0.14\beta_2)E_2, \\ \sigma_1 &= 3.84A/\Gamma_1, \\ \sigma_2 &= 1.464A^{4/3}/\Gamma_2. \end{aligned} \tag{2}$$

GDR parameters are crucial for fundamental problems of nuclear physics and studied widely for a long time. Researchers refer to experimental data taken from RIPL[5] database for photon-induced calculations. If experimental data are absent, GDR parameters are calculated by using the systematic equations given above. Photo-nuclear reaction cross-section calculations, very useful for radiation shielding in radiotherapy rooms, fundamental nuclear physics problems, astrophysics, etc., are an attractive research area and widely studied by researchers.[6–15]

Classification is a crucial machine learning method with broad applications. It is used to classify each item in a set of data into one of the predefined sets of classes or groups. Classifier selection considering the problem domain plays an

important role in more accurate classification results. In this research, we have analyzed Meta-Learning and Tree-based classifiers. AdaBoost and LogitBoost have been used as Meta classifiers, whereas ADTree and NBTree have been used as Tree classifiers.[16]

Boosting is often used to boost a weak classifier or learner to achieve with the purpose of achieving an accuracy classifier highly. In other words, boosting can be considered a meta-learning algorithm. The misclassified examples from the previous model are used to create an ensemble. The classifiers that are based on a decision tree with a root node and two leaf nodes such as a decision stump are often used as a boosting technique.[17] Various classification methods are proposed for classifiers such as the Tree-based model, Mixture model, Boosting, Bagging, etc.[18]

There have been many studies, carried out by using artificial neural network (ANN), for nuclear physics, and high-energy physics such as development of learning-based approaches in nuclear science,[19] GDR key parameters with multi-task neural networks,[20] GDR predictions,[21] mass excess estimations,[22] nuclear mass predictions based on Bayesian neural network,[23] predictions of nuclear β-decay half-lives with machine learning[24] and estimation of fusion reaction cross-sections by ANNs.[25] In the previous study, we also investigated the GDR parameters for spherical nuclei by using an ANN.[26]

In this study, we used LogitBoost meta-estimator with RandomTree classifier available in the Waikato Environment for Knowledge Analysis (WEKA) tool[27] for the classification of the deformed and spherical nuclei. The LogitBoost meta-estimator aims to minimize the logistic loss to create an additive model. It is mainly used for performing additive logistic regression. Then, we used an ANN, exactly with an Levenberg–Marquardt (LM) algorithm to estimate GDR parameters for deformed nuclei.

The application of LM to neural network training is described in Refs. 28 and 29. This algorithm is the fastest method for training moderate-sized feed forward neural networks up to several weights.[28,29] Also, photo-neutron cross-sections of $^{233}\mathrm{U}(\gamma,\mathrm{n})^{232}\mathrm{U}$, $^{234}\mathrm{U}(\gamma,\mathrm{n})^{233}\mathrm{U}$, $^{235}\mathrm{U}(\gamma,\mathrm{n})^{234}\mathrm{U}$, $^{236}\mathrm{U}(\gamma,\mathrm{n})^{235}\mathrm{U}$, $^{238}\mathrm{U}(\gamma,\mathrm{n})^{237}\mathrm{U}$ have been computed, with new GDR parameters, by using TALYS 1.95[30] code. TALYS is a powerful nuclear reaction code, widely used by researchers to compare theoretical results with experimental data.[31–40] Also, photo-neutron calculations have been redone by using systematic GDR parameters. The photo-neutron cross-sections obtained in this study have been compared with experimental data in this study.

2. Material and Methods

The LogitBoost classifier formulated by Jerome Friedman is a meta classifier based on the well-known AdaBoost.[41] It is a boosting algorithm that uses a regression scheme as the base learner and can handle multi-class problems.[17,42] LogitBoost replaces the exponential loss of AdaBoost algorithm with conditional Bernoulli

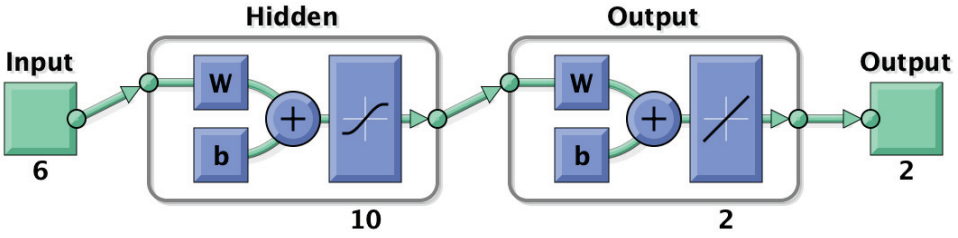


Fig. 1. The ANN connections for resonance energy.

likelihood loss. Specifically, if one considers AdaBoost as a generalized additive model and then applies the function of logistic regression, one can derive the LogitBoost algorithm. Therefore, the LogitBoost algorithm is used as an extension of AdaBoost algorithm.[41]

In the first part of the study, we evaluated the performances in terms of classification accuracy of meta-estimator with RandomTree classifier. It is also possible to observe both a deformed (nonspherical) and a spherical shape in 100 nuclei at different parameters via the LogitBoost algorithm. Thus, two different classes were distinguished from each other and tried to be determined with high accuracy (as class 0 (spherical nuclei) and class 1 (deformed nuclei)). In the second part of the study, we used ANN in MATLAB 2019b to estimate GDR parameters.

The LM algorithm is eminently conforming to training networks. It provides well performance of information for prediction which is compared to the backpropagation algorithm.[28,43,44] It is an iterative technique that locates a local minimum of a multi-variate function to express nonlinear least-squares problems for least-squares curve fitting especially. It can interpolate between the Gauss–Newton algorithm and (a combination of the steepest descent and the Gauss–Newton method).[45–47] The LM backpropagation algorithm is used for network training (correct weights as called network training). It processes on hidden layers and is sent to the output layer, which initially has correct values to correct assigned output weight. The training stops when generalization automatically stops enhancing, as indicated by an increase in mean square error (MSE) as the average squared difference between targets and outputs of validation models. Lower values are better, meaning zero errors. Regression (R) analysis is performed to measure the correlation between targets and outputs.[43,44,48]

In our proposed method, GDR parameters are obtained by using ANN which is trained with the LM backpropagation algorithm using MATLAB 2019b. The ANN topology of the proposed method for resonance energy has an input layer with six neurons for each of the mass number (A), proton number (Z), neutron number (N), the radius of nuclei, asymmetry term, and $((N-Z)\backslash N)$, a single hidden layer having 10 neurons and output layer having two neurons, as shown in Fig. 1. Sigmoid activation function is applied to a weighted sum of inputs, and the output is used as an input to the following layer.

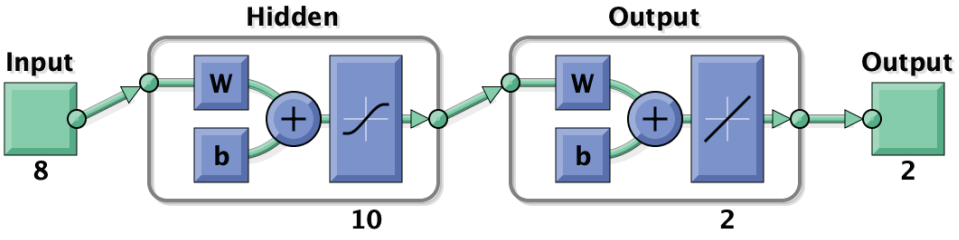


Fig. 2. The ANN connections for FWHM.

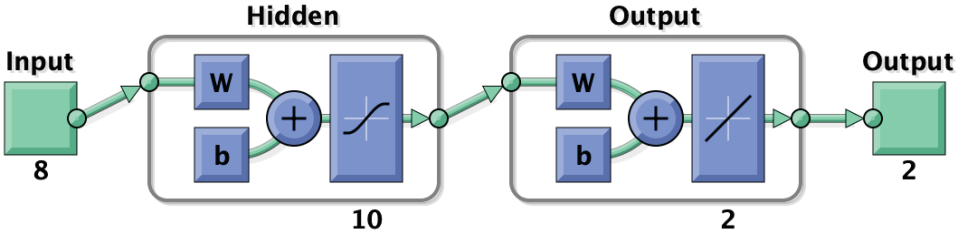


Fig. 3. The ANN connections for resonance cross-section.

When a neuron's activation function is a sigmoid function, the output of this unit will always be between 0 and 1. Furthermore, the sigmoid is a nonlinear function, the output of this unit is a nonlinear function of the weighted sum of inputs. A sigmoid unit is a neuron that uses a sigmoid function as an activation function. We used the logarithmic loss function to measure the noise coming from using a predictor as opposed to the true labels.[48]

Afterward, resonance energy results have been added to the input layer for FWHM and FWHM results have been added to the input layer for resonance cross-section estimations. The topology of ANN used to FWHM and resonance cross-section can be seen in Figs. 2 and 3. Detailed information on the ANN topology used in this paper can be found in Ref. 26.

$^{233}\mathrm{U}(\gamma,\mathrm{n})^{232}\mathrm{U}$, $^{234}\mathrm{U}(\gamma,\mathrm{n})^{233}\mathrm{U}$, $^{235}\mathrm{U}(\gamma,\mathrm{n})^{234}\mathrm{U}$, $^{236}\mathrm{U}(\gamma,\mathrm{n})^{235}\mathrm{U}$, $^{238}\mathrm{U}(\gamma,\mathrm{n})^{237}\mathrm{U}$ reaction cross-sections have been reproduced by using TALYS 1.95 with newly obtained GDR parameters. Also, GDR parameter library of TALYS 1.95 has been deactivated to compute the reaction cross-sections by using GDR parameters determined by systematic calculations. Default parameters have been used at TALYS 1.95 calculations except for GDR parameters.

3. Results and Discussion

We tested 100 different nuclei belonging to all GDR parameters within RIPL database, by using the classifier is deformed or not. This study evaluates the performances in terms of classification accuracy of the meta-estimator with RandomTree classifier that gives 100 nuclei in total for different classes. Two different classes,

Table 1. Statistical results obtained from LogitBoost.

Measure	Value
Instances	93%
Kappa statistic	0.8576
Mean absolute error	0.083
Root mean squared error	0.2659
Relative absolute error	16.9044%
Root relative squared error	53.6778%
Total Number of Instances	100

such as class 0 (spherical nuclei) and class 1 (deformed nuclei) which is 93% of test instances, were classified. The statistical results obtained from the LogitBoost algorithm are in Table 1. The kappa statistic value is much closer to 1 which provides a strong agreement for the classification of data. When our trained model is applied to the test data partition, accuracy is defined as the number of correctly classified instances divided by the total number of instances.

The formula to calculate Cohen's kappa for two raters is as given in the following equation:

$$\mathbb{K} = \frac{p_o - p_e}{1 - p_e}, \tag{3}$$

where p_o is the relative observed agreement among raters and p_e is the hypothetical probability of chance agreement.

In statistics, mean absolute error (MAE) is a measure of errors between paired observations expressing the same phenomenon, as shown in Eq. (4). For example, y_i versus x_i will include comparisons of predicted versus observed measurement.

$$\text{MAE} = \frac{\sum_{i=1}^{n} |y_i - x_i|}{n}. \tag{4}$$

MSE and MAE are used to assess the accuracy of the regression issue. The errors are squared before being averaged in root mean square error (RMSE). This means that RMSE gives larger mistakes a higher weight. Thus, RMSE is significantly more beneficial when substantial errors are present and have a significant impact on the model's performance, as shown in the following equation:

$$\begin{aligned} \text{MSE} &= \frac{1}{n}\sum_{i=1}^{n}(y_i - \bar{y}_i)^2, \\ \text{RMSE} &= \sqrt{\frac{1}{n}\sum_{i=1}^{n}(y_i - \bar{y}_i)^2}. \end{aligned} \tag{5}$$

The root relative squared error (RRSE) shows the difference between the model and a simple predictor based on averaged values. The relative absolute error (RAE)

is the total absolute error instead of the total squared error, as shown in the following equation:

$$\text{RAE} = \frac{\frac{1}{n}\sum_{i=1}^{n}(y_i - \hat{y}_i)}{\frac{1}{n}\sum_{i=1}^{n}(y_i - \bar{y})^2}. \tag{6}$$

The RRSE is defined as the square root of the sum of squared errors of a predictive model normalized by the sum of squared errors of a simple model, as shown in the following equation:

$$\text{RRSE} = \sqrt{\frac{\frac{1}{n}\sum_{i=1}^{n}(y_i - \hat{y}_i)}{\frac{1}{n}\sum_{i=1}^{n}(y_i - \bar{y})^2}}, \tag{7}$$

where n represents the number of observations, y_i represents the realized value, $\hat{y}_i$ represents the predicted value, and $\bar{y}$ represents the average of the realized values.

True Positive (TP) rate is instance correctly classified as a given class. False Positive (FP) rate is instance falsely classified as a given class. False Negative (FN) is a test result which wrongly indicates that a condition does not hold.

In Eq. (8), Recall (equivalent to TP rate) is the proportion of instances classified as a given class divided by the actual total in that class. Precision is the proportion of instances that are true of a class divided by the total instances classified as that class. F-Measure is a combined measure for Precision and Recall.

$$\begin{aligned} \text{Recall} &= \frac{\text{TP}}{\text{TP} + \text{FN}}, \\ \text{Precision} &= \frac{\text{TP}}{\text{TP} + \text{FP}}, \\ \text{F-Measure} &= \frac{2 * \text{Precision} * \text{Recall}}{\text{Precision} + \text{Recall}}. \end{aligned} \tag{8}$$

First, class 0 accuracy of TP rate is 0.930, FP rate is 0.070, Precision is 0.946, Recall is 0.930, and F-Measure is 0.938 value. Second, class 1 accuracy of TP rate is 0.930, FP rate is 0.070, Precision is 0.909, Recall is 0.930, and F-Measure is 0.920 value. The weighted average accuracy for the two-class using LogitBoost classifier such as TP rate is 0.930, FP rate is 0.070, Precision is 0.930, Recall is 0.930, and F-Measure is 0.930 for weighted average. The more exact results for all 100 nuclei for two different classes using accuracy evaluation are presented in Table 2.

Table 2. Weighted average accuracies for the two-class using LogitBoost classifier.

Class	TP rate	FP rate	Precision	Recall	F-Measure
0	0.930	0.070	0.946	0.930	0.938
1	0.930	0.070	0.909	0.930	0.920
Weighted av.	0.930	0.070	0.930	0.930	0.930

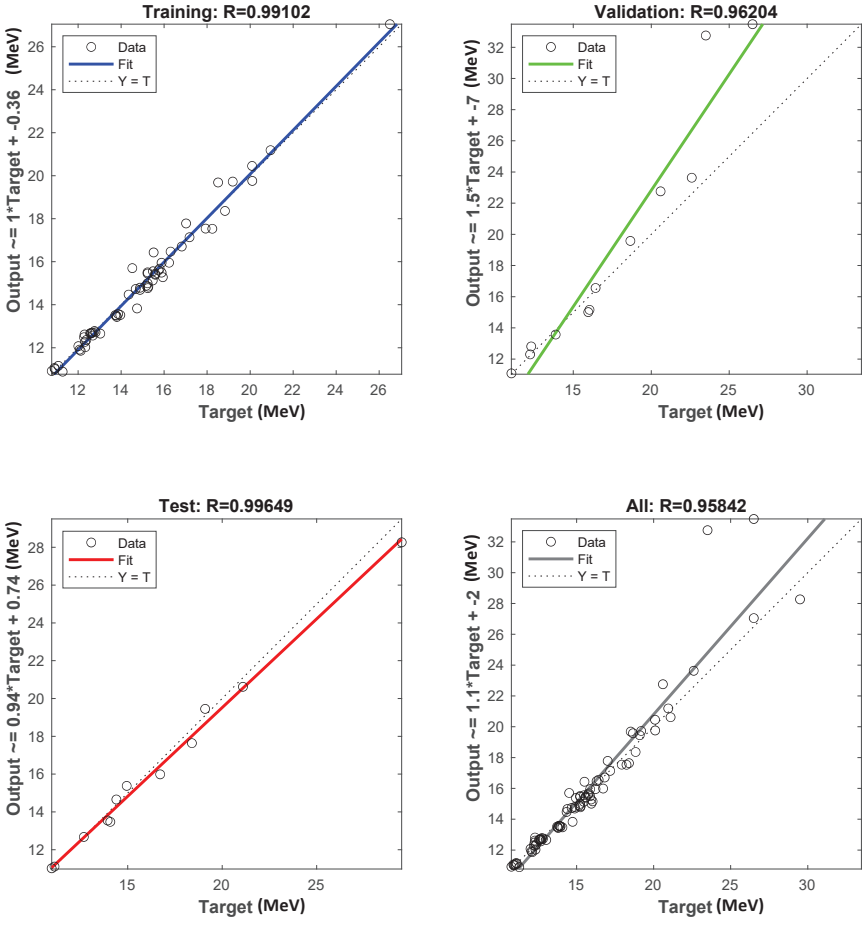


Fig. 4. (Color online) The ANN estimations for resonance energy.

We have determined that ^{233}U, ^{234}U, ^{235}U, ^{236}U, and ^{238}U isotopes have two GDR peaks. After the classification, the RIPL data are reserved for validation, testing, and training to estimate GDR parameters of deformed nuclei. The data, such as validation, test, and training, were set to 15%, 15%, and 70%, respectively. The motivation of this paper is to establish an ANN algorithm, which can be used in the lack of experimental data, for GDR parameters belonging to deformed nuclei. Resonance cross-sections data used in this study, shown in Figs. 3 and 6, belong to photo-absorption reactions. RIPL data were obtained by a fit of the theoretical photo-absorption cross-sections to the experimental data. The obtained results are presented in Figs. 4–6. Furthermore, GDR parameters obtained by using ANN have been presented in Table 3.

The performance of ANN estimates is demonstrated using MSE results. MSE results of the ANN estimations have been presented in Table 4.

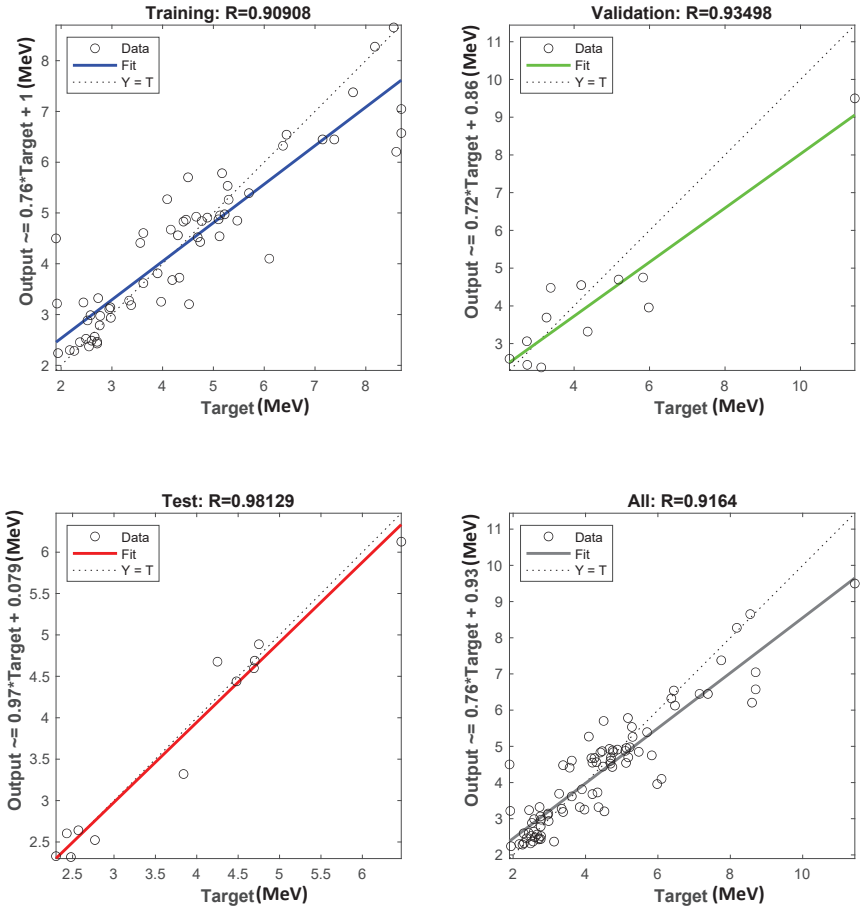


Fig. 5. (Color online) The ANN estimations for FWHM.

RMSE values of theoretical model results and ANN estimations have been given in Table 5. Theoretical results have been obtained by combining RIPL theoretical results with Eq. (2). As can be seen in Table 5, ANN estimations are more successful than theoretical approximations.

The target represents experimental data obtained from RIPL database, whereas output refers to the estimation results of ANN in all ANN estimation figures. The ANN estimations for resonance energy have been presented in Fig. 4. R values of training, estimation, and testing processes have been found 0.99102, 0.96204, and 0.99649, respectively, as seen in Fig. 4. R values of all processes have been determined as 0.95842. In Fig. 5, FWHM estimations have been shown. Correlation results have been obtained as 0.90908, 0.93498, 0.98129, and 0.9164 for training, validation, testing, and all process, respectively. The ANN estimations for resonance cross-section have been presented in Fig. 6. R values of training, estimation, and

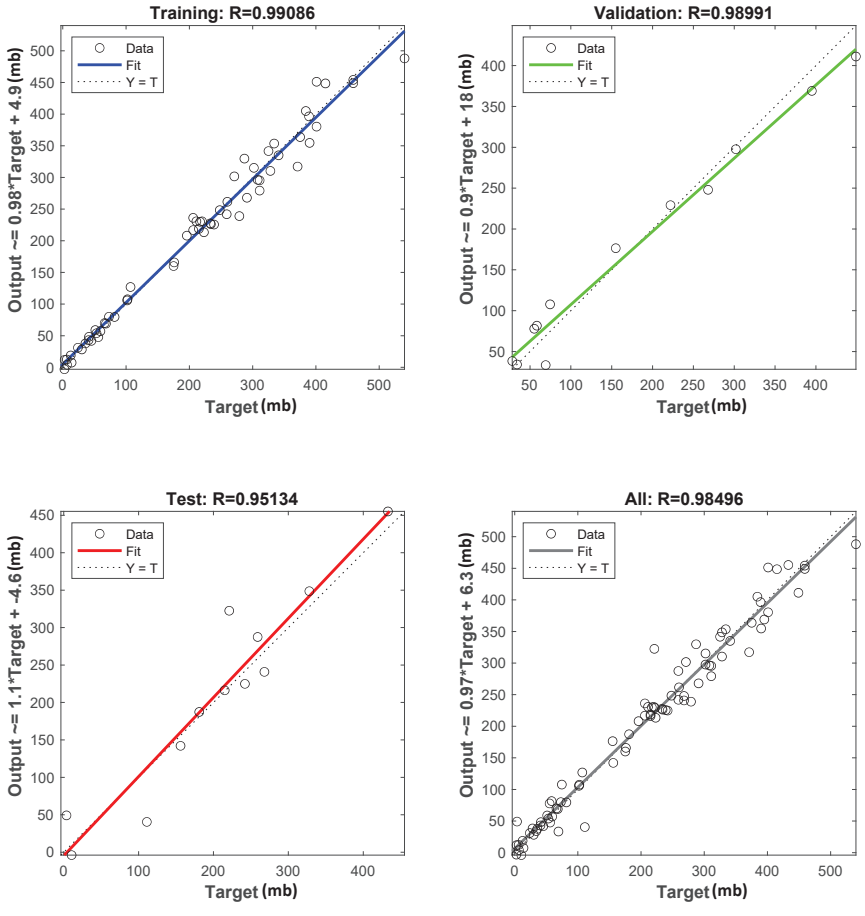


Fig. 6. (Color online) The ANN estimations for resonance cross-section.

testing process have been found 0.99086, 0.98991, and 0.95134, respectively. Also, R values of all processes have been determined as 0.98496.

In addition to ANN estimations, $^{233}\mathrm{U}(\gamma,\mathrm{n})^{232}\mathrm{U}$, $^{234}\mathrm{U}(\gamma,\mathrm{n})^{233}\mathrm{U}$, $^{235}\mathrm{U}(\gamma,\mathrm{n})^{234}\mathrm{U}$, $^{236}\mathrm{U}(\gamma,\mathrm{n})^{235}\mathrm{U}$, $^{238}\mathrm{U}(\gamma,\mathrm{n})^{237}\mathrm{U}$ reaction cross-sections have been reproduced via TALYS 1.95 code to validate ANN estimation. Two different calculations have been performed in TALYS code. First, TALYS GDR Database has been changed with our ANN estimations and then photo-neutron cross-sections have been done by using the systematical approximation of GDR parameters like Eq. (2). For calculations of GDR parameters obtained by ANN estimations, uranium isotopes' GDR parameters, which belong to the testing set, were embedded in TALYS 1.95 code and photo-neutron cross-section calculations were done. There are two options to change GDR parameters in TALYS nuclear reaction code. One is to specify the new GDR parameters in the input file, and the other is to change the GDR parameters

Table 3. GDR parameters found by the ANN estimation.

Isotope	E_1 (MeV)	E_2 (MeV)	Γ_1 (MeV)	Γ_2 (MeV)	σ_1 (mb)	σ_2 (mb)
^{152}Sm	12.36	15.60	3.14	4.97	165.77	226.26
^{154}Sm	12.49	15.28	3.11	5.39	187.35	216.22
^{153}Eu	12.02	15.68	3.06	4.75	176.46	229.15
^{160}Gd	12.30	15.01	2.97	5.53	218.72	227.51
^{159}Tb	11.91	15.49	2.94	4.87	208.04	248.37
^{165}Ho	12.07	15.39	2.89	4.54	225.60	267.92
^{166}Er	11.86	15.44	2.79	4.43	224.87	287.48
^{175}Lu	12.27	15.13	2.64	4.69	229.91	329.75
^{181}Ta	12.61	15.00	2.60	4.44	241.90	335.01
^{184}W	12.67	14.88	2.56	4.52	240.89	348.64
^{186}W	12.66	14.69	2.60	4.70	230.72	353.60
^{187}Re	12.69	14.77	2.52	4.60	238.94	363.78
^{186}Os	12.66	14.84	2.37	4.48	296.17	315.17
^{188}Os	12.72	14.79	2.44	4.55	261.55	354.68
^{189}Os	12.71	14.73	2.46	4.61	247.91	369.01
^{190}Os	12.67	14.66	2.49	4.67	236.19	380.36
^{192}Os	12.57	14.47	2.52	4.83	216.80	396.49
^{232}Th	11.08	13.57	2.43	4.84	297.63	411.18
^{233}U	11.16	13.57	2.24	4.85	322.49	455.19
^{234}U	11.11	13.55	2.28	4.87	317.22	451.24
^{235}U	11.06	13.52	2.33	4.89	310.30	448.95
^{236}U	11.01	13.49	2.37	4.91	301.69	448.54
^{238}U	10.92	13.43	2.46	4.95	279.24	454.17
^{237}Np	11.02	13.47	2.30	4.93	295.52	488.08
^{239}Pu	10.89	13.52	2.32	4.68	341.71	405.04
^{12}C	23.63	33.48	4.50	6.21	12.34	−3.03
^{14}N	22.76	32.75	4.56	5.70	11.90	7.40
^{27}Al	20.62	28.27	4.10	6.57	18.77	4.06
v^{28}Si	19.76	27.05	3.81	7.05	−3.83	49.18
^{51}V	17.54	21.19	3.62	6.45	53.93	43.00
^{55}Mn	16.71	20.46	3.73	5.27	58.88	41.86
^{59}Co	16.56	19.58	3.32	6.45	38.36	81.59
^{60}Ni	16.47	19.69	3.24	6.32	34.09	77.86
^{63}Cu	15.99	19.45	3.68	4.41	69.95	28.25
^{64}Zn	15.95	19.73	3.69	3.96	48.24	47.65
^{74}Ge	15.70	17.78	3.22	8.27	31.01	107.53
^{76}Ge	16.43	18.36	3.32	9.50	57.11	79.96
^{75}As	15.45	17.53	3.20	7.38	33.41	107.76
^{76}Se	15.38	17.64	3.32	6.13	69.07	79.58
^{78}Se	15.51	17.14	2.99	8.65	37.73	105.74
^{127}I	13.83	15.95	3.27	6.54	40.49	142.09
^{148}Nd	12.78	15.56	3.25	5.26	126.91	230.71
^{150}Nd	12.81	15.16	3.18	5.78	160.05	213.42

for the target nuclei in the structure file of TALYS code. Cross-section calculations of ^{233}U$(\gamma,\mathrm{n})^{232}$U, ^{234}U$(\gamma,\mathrm{n})^{233}$U, ^{235}U$(\gamma,\mathrm{n})^{234}$U, ^{236}U$(\gamma,\mathrm{n})^{235}$U, ^{238}U$(\gamma,\mathrm{n})^{237}$U reactions have been shown in Figs. 7–11.

Figure 7 shows the comparison of ^{233}U$(\gamma,\mathrm{n})^{232}$U reaction cross-sections with experimental data of de Moraes and Cesar[49] and Berman *et al.*[50] The experimental

Table 4. MSE results of the ANN estimations.

E_1 (MeV)	E_2 (MeV)	Γ_1 (MeV)	Γ_2 (MeV)	σ_1 (mb)	σ_2 (mb)
0.26	3.38	0.46	0.75	686	478

Table 5. RMSE results of the ANN estimations and theoretical results.

	E_1 (MeV)	E_2 (MeV)	Γ_1 (MeV)	Γ_2 (MeV)	σ_1 (mb)	σ_2 (mb)
ANN estimations	0.37	0.48	0.48	0.67	27.34	21.74
Theoretical results	0.39	0.52	0.77	1.12	38.07	54.92

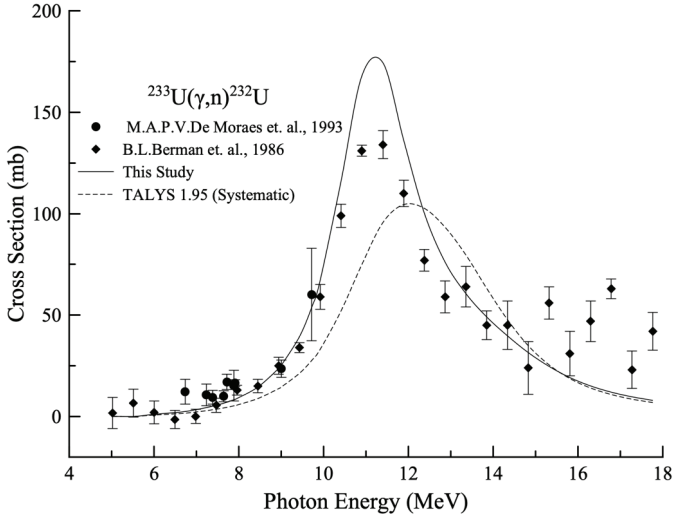


Fig. 7. The comparisons of the $^{233}\mathrm{U}(\gamma,\mathrm{n})^{232}\mathrm{U}$ reaction cross-section calculations with experimental data.

data contain proton contribution after 13 MeV photon energy, but calculations have been done an only the photo-neutron reaction. ANN results have consisted of experimental data except for peak cross-section value. Estimation of resonance cross-section is the reason for this mismatch.

As can be seen in Fig. 7, reaction cross-section calculations, done with ANN estimations, are better in agreement with the experimental data than systematic calculations.

In Fig. 8, photo-neutron cross-section calculations for $^{234}\mathrm{U}(\gamma,\mathrm{n})^{233}\mathrm{U}$ reaction have been presented. The experimental data of Berman *et al.*,[50] have been used to compare theoretical calculations. Photo-neutron calculations performed by using GDR parameters found by ANN estimations are in well-matched with experimental data in terms of geometrical shape. ANN calculations give higher values for peak cross-section whereas systematic calculations have shifted to the right.

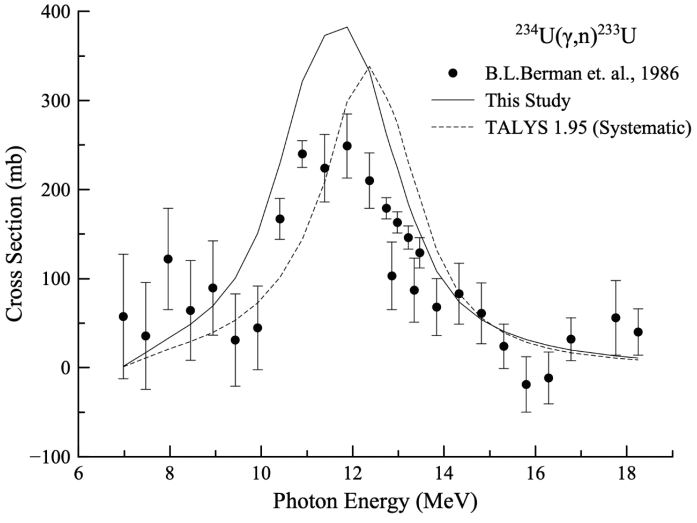


Fig. 8. The same as Fig. 7, but for the $^{234}\mathrm{U}(\gamma,\mathrm{n})^{233}\mathrm{U}$ reaction.

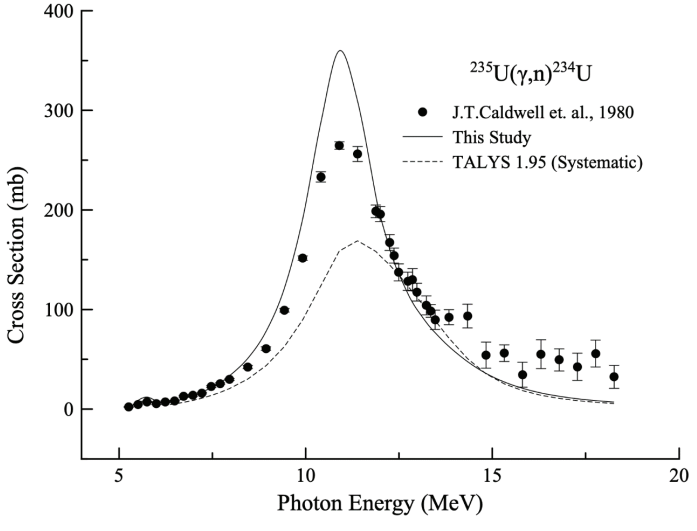


Fig. 9. The same as Fig. 7, but for the $^{235}\mathrm{U}(\gamma,\mathrm{n})^{234}\mathrm{U}$ reaction.

$^{235}\mathrm{U}(\gamma,\mathrm{n})^{234}\mathrm{U}$ reaction cross-section calculations versus experimental data of Caldwell *et al.*,[51] have been shown in Fig. 9. Both calculations have exhibited similar geometry with Ref. 51. However, systematic calculations have been given lower cross-section results than experimental data. ANN calculations have been found better than systematic calculations. Figure 10 shows the comparison of $^{236}\mathrm{U}(\gamma,\mathrm{n})^{235}\mathrm{U}$ reaction cross-sections with experimental data of Caldwell *et al.*[51]

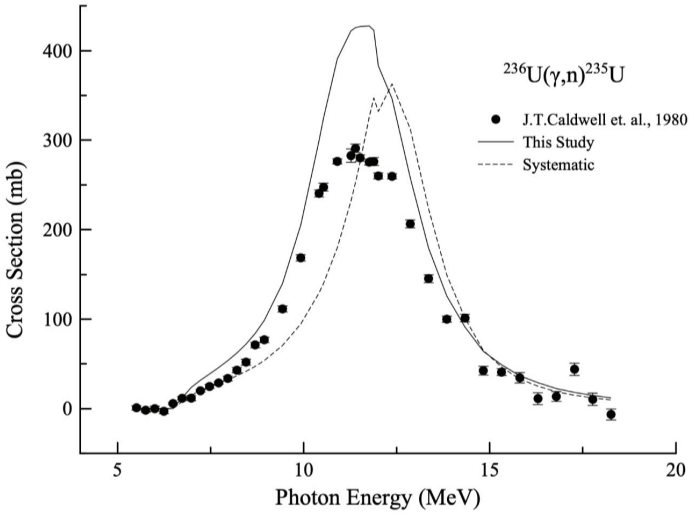


Fig. 10. The same as Fig. 7, but for the $^{236}\mathrm{U}(\gamma, \mathrm{n})^{235}\mathrm{U}$ reaction.

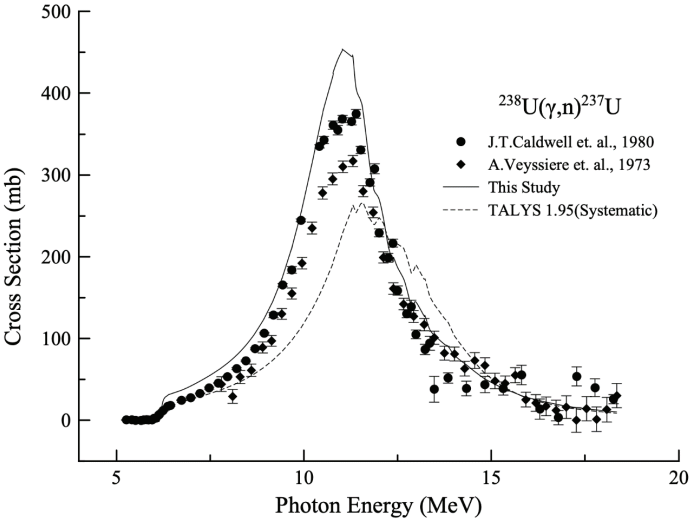


Fig. 11. The same as Fig. 7, but for the $^{238}\mathrm{U}(\gamma, \mathrm{n})^{237}\mathrm{U}$ reaction.

ANN calculations have exhibited close geometry with experimental data whereas systematic calculations have shifted to the right. In Fig. 11, $^{238}\mathrm{U}(\gamma, \mathrm{n})^{237}\mathrm{U}$ reaction cross-section calculations against experiments of Caldwell *et al.*,[51] and Veyssière *et al.*,[52] have been presented. Systematic calculations have been shifted toward the right which are the results of FWHM values. ANN results have been found to be better than the systematic calculations.

4. Conclusions

In this study, we focused on estimating GDR parameters for deformed nuclei. For this purpose, first, all nuclei, whose GDR parameters exist in the RIPL database, have been classified as spherical and deformed by using WEKA. The performances are evaluated in terms of classification accuracy of LogitBoost meta-estimator with RandomTree classifier, which gives 100 nuclei in total for two classes. It has been found that ^{233}U, ^{234}U, ^{235}U, ^{236}U, and ^{238}U have two humps. After that, GDR parameters of deformed nuclei have been estimated by using ANN. In the last step, photo-neutron cross-sections of ^{233}U, ^{234}U, ^{235}U, ^{236}U, and ^{238}U isotopes have been calculated by using two sets of GDR parameters, which are found by ANN estimations and systematic calculations. Obtained results can be summarized as follows: the LogitBoost classifier using the AdaBoost procedure to estimate the deformed nuclei by WEKA 3.9.4.

The GDR parameters estimated via ANN models with LM are more effective than systematic calculations and resonance energy estimations should be modified. Therefore, the R values of ANN estimations have been found as 0.96, 0.92, and 0.99 for resonance energy, FWHM, and resonance cross-section, respectively. In the absence of experimental data, neural networks should be the first method to calculate GDR parameters for deformed nuclei. According to the results of MSE, RMSE and R were determined the best result as ANN estimations (Table 5 and Figs. 4–6). The photo-neutron cross-section calculations which have been carried out by using GDR parameters from ANN are found to be more successful than the calculations using GDR parameters determined by systematic calculations. Future studies should be done by using deformation parameters for deformed and spherical nuclei.

References

1. M. Goldhaber and E. Teller, *Phys. Rev.* **74**, 1046 (1948).
2. H. Steinwedel and J. D. Jensen, *Z. Naturforsch. A* **5**, 413 (1950).
3. D. Santonocito and Y. Blumenfeld, *Eur. Phys. J. A*: *Hadrons Nuclei* **30**, 183 (2006).
4. M. Herman, R. Capote, B. Carlson, P. Obložinský, M. Sin, A. Trkov, H. Wienke and V. Zerkin, *Nucl. Data Sheets* **108**, 2655 (2007).
5. R. Capote, M. Herman, P. Obložinský, P. Young, S. Goriely, T. Belgya, A. Ignatyuk, A. Koning, S. Hilaire, V. Plujko, M. Avrigeanu, O. Bersillon, M. Chadwick, T. Fukahori, Z. Ge, Y. Han, S. Kailas, J. Kopecky, V. Maslov, G. Reffo, M. Sin, E. Soukhovitskii and P. Talou, *Nucl. Data Sheets* **110**, 3107 (2009).
6. M. Şekerci, H. Özdoğan and A. Kaplan, *Radiochim. Acta* **108**, 11 (2020).
7. H. Özdoğan, M. Şekerci and A. Kaplan, *Appl. Radiat. Isot.* **143**, 6 (2019).
8. H. Özdoğan, M. Şekerci and A. Kaplan, *Phys. At. Nucl.* **82**, 324 (2019).
9. H. Özdoğan, M. Şekerci and A. Kaplan, *Appl. Radiat. Isot.* **165**, 109356 (2020).
10. A. Kaplan, H. Özdoğan, A. Aydın and E. Tel, *J. Fusion Energy* **32**, 97 (2013).
11. A. Kaplan, H. Özdoğan, A. Aydın and E. Tel, *J. Fusion Energy* **32**, 344 (2013).
12. A. Kaplan, M. Şekerci, V. Çapalı and H. Özdoğan, *J. Fusion Energy* **36**, 213 (2017).
13. A. Kaplan, H. Özdoğan, A. Aydın and E. Tel, *Phys. At. Nucl.* **77**, 1371 (2014).

14. I. H. Sarpün, H. Özdoğan, K. Taşdöven, H. A. Yalim and A. Kaplan, *Mod. Phys. Lett. A* **34**, 1950210 (2019).
15. E. Vagena and S. Stoulos, *Eur. Phys. J. A* **53**, 85 (2017).
16. M. Panda and M. R. Patra, Ensembling rule based classifiers for detecting network intrusions, in *Int. Conf. Advances in Recent Technologies in Communication and Computing* (*ARTCom 2009*) (IEEE Computer Society, 2009), pp. 19–22.
17. W. Hu, W. Hu and S. Maybank, *IEEE Trans. Syst. Man Cybern. B*: *Cybern.* **38**, 577 (2008).
18. S. Fakhraei, H. Soltanian-Zadeh and F. Fotouhi, *Expert Syst. Appl.* **41**, 6945 (2014).
19. M. Fernandez, K. Higley, A. Tokuhiro, K. Welter, W. Wong and H. Yang, *Nucl. Eng. Des.* **359**, 1 (2019).
20. J. Bai, Z. Niu, B. Sun and Y. Niu, *Phys. Lett. B* **815**, 136147 (2021).
21. X. Wang, L. Zhu and J. Su, *Phys. Rev. C* **104**, 034317 (2021).
22. H. Özdoğan, Y. Üncü, M. Şekerci and A. Kaplan, *Appl. Radiat. Isot.* **184**, 110162 (2022).
23. Z. Niu and H. Liang, *Phys. Lett. B* **778**, 48 (2018).
24. Z. M. Niu, H. Z. Liang, B. H. Sun, W. H. Long and Y. F. Niu, *Phys. Rev. C* **99**, 064307 (2019).
25. S. Akkoyun, *Nucl. Instrum. Methods Phys. Res. B* **462**, 51 (2020).
26. H. Özdoğan, Y. A. Üncü, O. Karaman, M. Şekerci and A. Kaplan, *Appl. Radiat. Isot.* **169**, 109581 (2021).
27. I. H. Witten and E. Frank, *SIGMOD Rec.* **31**, 76 (2002).
28. M. Hagan and M. Menhaj, *IEEE Trans. Neural Netw.* **5**, 989 (1994).
29. B. G. Kermani, S. S. Schiffman and H. T. Nagle, *Sens. Actuators B*: *Chem.* **110**, 13 (2005).
30. A. Koning, S. Hilaire and M. Duijvestijn, NRG-1755 ZG Petten, The Netherlands (2019).
31. M. Şekerci, H. Özdoğan and A. Kaplan, *Mosc. Univ. Phys. Bull.* **74**, 277 (2019).
32. E. Vagena and S. Stoulos, *HNPS Adv. Nucl. Phys.* **24**, 123 (2019).
33. M. Sadeghi, M. Aboudzadeh, A. Zali and B. Zeinali, *Appl. Radiat. Isot.* **67**, 1392 (2009).
34. M. Sadeghi, M. Enferadi and H. Nadi, *J. Radioanal. Nucl. Chem.* **286**, 259 (2010).
35. M. Sadeghi and M. Enferadi, *Ann. Nucl. Energy* **38**, 825 (2011).
36. M. Sadeghi, A. Zali, M. Aboudzadeh, P. Sarabadani, G. Aslani and A. Majdabadi, *Appl. Radiat. Isot.* **67**, 2029 (2009).
37. M. Sadeghi, N. Zandi and M. Bakhtiari, *J. Radioanal. Nucl. Chem.* **292**, 777 (2012).
38. M. Sadeghi, T. Kakavand and Z. Alipoor, *Mod. Phys. Lett. A* **25**, 1541 (2010).
39. A. K. M. R. Rahman and M. A. Zubair, *Indian J. Phys.* **95**, 1231 (2021).
40. S. Harissopulos, E. Vagena, M. Axiotis,, A. Spyrou, G. Provatas, A. Lagoyannis, P. Dimitriou and H. Becker, *EPJ Web Conf.* **227**, 01008 (2020).
41. J. Friedman, T. Hastie and R. Tibshirani, *Ann. Stat.* **28**, 337 (2000).
42. Y. Freund and R. E. Schapire, *J. Comput. Syst. Sci.* **55**, 119 (1997).
43. J. J. Hopfield, *Proc. Natl. Acad. Sci. USA* **79**, 2554 (1982).
44. R. Rojas, *Neural Networks*: *A Systematic Introduction* (Springer-Verlag, 1996).
45. K. Levenberg, *Q. Appl. Math.* **2**, 164 (1944).
46. B. M. Wilamowski and H. Yu, *IEEE Trans. Neural Netw.* **21**, 930 (2010).
47. J.-M. Wu, *IEEE Trans. Neural Netw.* **19**, 2032 (2008).
48. D. E. Rumelhart, G. E. Hinton and R. J. Williams, *Nature* **323**, 533 (1986).
49. M. A. P. V. de Moraes and M. F. Cesar, *Nuovo Cimento A* **106**, 1165 (1993).

50. B. L. Berman, J. T. Caldwell, E. J. Dowdy, S. S. Dietrich, P. Meyer and R. A. Alvarez, *Phys. Rev. C* **34**, 2201 (1986).
51. J. T. Caldwell, E. J. Dowdy, B. L. Berman, R. A. Alvarez and P. Meyer, *Phys. Rev. C* **21**, 1215 (1980).
52. A. Veyssière, H. Beil, R. Bergere, P. Carlos, A. Lepretre and K. Kernbath, *Nucl. Phys. A* **199**, 45 (1973).